16th European Signal Processing Conference (EUSIPCO 2008), Lausanne, Switzerland, August 25-29, 2008, copyright by EURASIP

COLOR DEMOSAICING USING MULTI-FRAME SUPER-RESOLUTION

Mejdi Trimeche

Media Technologies Laboratory
Nokia Research Center, Tampere, Finland
email: mejdi.trimeche@nokia.com

ABSTRACT

Despite the considerable advances in the fabrication processes of imaging sensors, their performance remains limited by theoretical constraints that compromise the achievable sensitivity, frame rate, signal to noise ratio, pixel size and spatial resolution. Therefore, signal processing techniques are needed to improve the final image quality. In this paper, we present a framework for producing a high-resolution color image directly from a sequence of images captured by a CMOS sensor that is overlaid with a color filter array. The method is based on iterative super-resolution that separately filters the color image planes, interpolates and combines these into a single output image. We present experimental results using synthetic image sequence as well as real data from CMOS sensors. The results confirm the potential of this technique to achieve superior image quality.

1. INTRODUCTION

Lately, the industry trend has been focusing on reducing the pixel size in order to improve the spatial resolution. This approach leads to reduced sensitivity of the individual pixels and results in the amplification of the noise levels because the performance of CMOS sensors is limited by low quantum efficiency and by dark current non-uniformity [6]. In fact, regardless of the sensor manufacturing technology, there is a fundamental trade-off between spatial sampling (number of pixels), pixel size, and temporal sampling.

Most consumer cameras consist of a single imaging sensor that uses Color Filter Arrays (CFA) to sample different spectral components. The sampling pattern is called the Bayer-matrix (Fig. 1), and consists of color filter elements arranged such that the green component is half the total number of pixels and twice the red and blue pixels. At each pixel location, the missing colors must be interpolated from neighboring samples. Color Filter Array Interpolation (CFAI), also known as demosaicing, is one of the most important tasks in the image formation pipeline of digital camera systems. A good review of demosaicing techniques can be found in [16]. Besides the traditional interpolation techniques such as nearest-neighbor replication, bilinear interpolation, and cubic spline interpolation; several advanced algorithms have been proposed in the literature. For example, in [2], [9] and [5], inter-channel correlation is exploited in various ways to perform edge-directed interpolation and to prevent color mismatch across the edges. In [8], a technique using alternating projections onto convex sets is proposed. The performance was superior to earlier techniques because the projections across the color planes provided for an efficient way to exploit inter-channel correlation. In [12], A unified camera image processing system that performs zooming and full color image reconstruction from single Bayer images is proposed, the CFA zooming is performed before interpolation so as to reduce the overall computational complexity and avoid the amplification of distracting artifacts. In all of the methods cited above, only the spatial correlation of the neighboring pixels is used, without exploiting the additional information that is available in the adjacent frames.

Super-resolution (SR) [1], [10], [3], [7], [17] is considered to be one of the most promising techniques that can help overcome the limitations due to optics and sensor resolution. The technique consists in combining a set of low-resolution (LR) images portraying slightly different views of the same scene in order to reconstruct a high-resolution (HR) image of that scene. In principle, super-resolution can be used to improve the performance of color demosaicing by combining a short sequence of raw images from the sensor and exploiting the non-redundant color samples that fall on different locations of the Bayer sampling lattice. To date, almost all super-resolution methods have been designed to increase the resolution of a single monochromatic channel (usually the luminance component), and it was not until recently that the use of multi-frame processing was considered in the problem of demosaicing ([11], [13], [14]). In [11], a method based on MAP estimation is proposed to jointly perform demosaicing and super-resolution, but the paper does not address the problem of estimating motion between the images, and only presents results with synthetic data sets. In [13] and [14], it is argued that although a two-pass algorithm (demosaicing followed by super-resolution) improves the overall resolution, this approach results in blurring effects and artifacts similar to those observed in demosaiced images. Also, they have shown that it is possible to obtain precise motion using block matching from aliased raw images. However, the overall method is complicated, and involves among other processing steps edge directed interpolation. Therefore, it is not straight-forward to separate the distinct contribution of super-resolution in the final demosaiced result. In [18], a Fourier domain algorithm that performs demosaicing and super-resolution jointly from a set of raw images was proposed. It was observed through experiments that the performance of the algorithm was very similar to the results obtained by applying demosaicing and super-resolution separately [18]; however it is not clear if the same observation is applicable to other spatial domain techniques.

1.1 Our approach

In earlier work [15], we have demonstrated that by applying deblurring directly on the raw color components, we were capable of producing superior results, especially after using simple checks to avoid color mismatch. In the following, we apply super-resolution directly on a sequence of raw images from the sensor. The idea is to enhance the interpolation of

the different color planes by utilizing the data from neighboring image frames. In Section 2, the image formation model is defined and in Section 3, we derive the solution by applying super-resolution on the color components. In Section 4, we highlight some implementation issues of the algorithm. In Section 5, we show experimental results with synthetic image data set and with real sensor data. Finally, we draw conclusions in Section 6.

2. IMAGE FORMATION MODEL

Consider a sequence of N raw LR images $(g_i, i = 1 \cdots N)$ that are captured directly from the sensor. The images are adjacent observations of a static scene corresponding to a HR color image (f). Further, each LR image g_i is composed of 4 color channels $g_{i(c)}$, where the index $c = \{1,2,3,4\}$ denotes respectively the data of the *Green1*, *Red*, *Blue*, and *Green2* color channels as measured according to the Bayer sampling pattern (Fig. 1). Using the notation above, the image formation model can be written as:

$$\begin{aligned} g_{i(1)}(x,y) &= S\downarrow\Big(h_{(1)} * f_G(\xi_i)\Big)(x,y) + \eta_{(1)}(x,y) \\ g_{i(2)}(x,y) &= S\downarrow\Big(h_{(2)} * f_R(\xi_i)\Big)(x,y) + \eta_{(2)}(x,y) \\ g_{i(3)}(x,y) &= S\downarrow\Big(h_{(3)} * f_B(\xi_i)\Big)(x,y) + \eta_{(3)}(x,y) \\ g_{i(4)}(x,y) &= S\downarrow\Big(h_{(4)} * f_G(\xi_i)\Big)(x,y) + \eta_{(4)}(x,y) \end{aligned} \quad (1)$$

where $f = (f_R, f_G, f_B)$ is the HR reference image corresponding to the imaged scene in the RGB domain. $h_{(c)}$ denotes the point spread function, or the PSF due to optical blurring in each color channel, $*$ denotes the convolution operator, and $S\downarrow$ the down-sampling operator. Note that in equation (1) each color component is subsampled at a different offset due to the specific pattern of the Bayer sampling matrix. ξ_i is the mapping function corresponding to the geometric warping due to the scene displacement in each of the LR images relative to the HR image f, while $\eta_{(c)}$ is an additive Gaussian noise term that corrupts each color channel.

After discretization, the model can be expressed in matrix form as follows:

$$\begin{aligned} \overline{g}_{i(1)} &= \mathbf{A}_{i(1)}\overline{f}_G + \overline{\eta}_{(1)} \\ \overline{g}_{i(2)} &= \mathbf{A}_{i(2)}\overline{f}_R + \overline{\eta}_{(2)} \\ \overline{g}_{i(3)} &= \mathbf{A}_{i(3)}\overline{f}_B + \overline{\eta}_{(3)} \\ \overline{g}_{i(4)} &= \mathbf{A}_{i(4)}\overline{f}_G + \overline{\eta}_{(4)} \end{aligned} \quad (2)$$

The matrix $\mathbf{A}_{i(c)}$ combines successively, the geometric transformation ξ_i, the convolution operator with the blurring parameters of $h_{(c)}$, and the down-sampling operator $S\downarrow$ over the Bayer grid. For notation convenience, we integrate the RGB correspondence in matrices $\mathbf{A}_{i(c)}$, and we express the image model using the following equation:

$$\overline{g}_{i(c)} = \mathbf{A}_{i(c)}\overline{f} + \overline{\eta}_{(c)} \quad (3)$$

where $\overline{g}_{i(c)}$, $\overline{f}$ and $\overline{\eta}_{(c)}$ are lexicographically ordered.

Referring to equation (3), the size of each of the LR images $\overline{g}_{i(c)}$ is quarter the size of the sensed raw image. The separation of the original image data into 4 subsampled images introduces aliasing since for each color plane we are skipping the pixels from the next color component without low-pass filtering. In principle, super-resolution algorithms can be particularly useful here since they exploit the aliasing in the interpolation process.

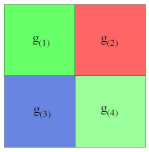

Figure 1: Bayer matrix sampling pattern

3. SUPER-RESOLUTION FROM RAW SENSOR DATA

In this section, we describe the algorithm that performs simultaneously the demosaicing of the color components while fusing the data from the LR frames. The HR image is in RGB domain, while the individual LR images are assumed to be the monochrome components after subsampling according to the Bayer pattern. The problem of super-resolution reconstruction can be described as estimating for each color channel the best HR image $\overline{f} = \left(\overline{f}_R, \overline{f}_G, \overline{f}_B\right)$, which when appropriately projected and down-sampled by the model in (2) will generate the closest estimates of the LR images $\overline{g}_{i(c)}$, $c = \{1 \cdots 4\}$.

For each observation $\overline{g}_{i(c)}$, we associate the following cost function:

$$\varepsilon_{i(c)} = ||\widehat{g}_{i(c)} - \overline{g}_{i(c)}||^2 = ||\mathbf{A}_{i(c)}\overline{f} - \overline{g}_{i(c)}||^2, \quad (4)$$

where $\widehat{g}_{i(c)}$ is the simulated LR image through the forward imaging model. If all LR images $(i = 1 \cdots N)$ are assumed to contribute equally to the cost function, then the overall cost function is the following:

$$\varepsilon_{(c)} = \sum_{i=1}^{N} \varepsilon_{i(c)} = \sum_{i=1}^{N} ||\mathbf{A}_{i(c)}\overline{f} - \overline{g}_{i(c)}||^2 \quad (5)$$

We use the method of iterative gradient descent to solve for the least squares solution by minimizing the cost function in (5). This technique seeks to converge $\varepsilon_{(c)}$ towards a local minimum by following the trajectory of the negative gradient; i.e., at iteration n, the high-resolution image is updated as follows:

$$\overline{f}^{n+1} = \overline{f}^{n} + \mu^n \overline{r}^n_{(c)}, \quad (6)$$

where μ^n is the step-size, and $\overline{r}^n_{(c)}$ is the residual gradient due to the LR color images (c).
The residual gradient $\overline{r}^n_{(c)}$ is computed as follows:

$$\overline{r}^n_{(c)} = \sum_{i=1}^{N} \mathbf{W}_{i(c)} \left(\overline{g}_{i(c)} - \mathbf{A}_{i(c)}\overline{f}^n\right). \quad (7)$$

The matrix $\mathbf{W}_{i(c)}$ corresponds to $\mathbf{A}^{(-1)}_{i(c)}$, i.e., the inverse process of the image formation. In practice, $\mathbf{W}_{i(c)}$ combines successively the up-sampling and the inverse geometric warp (ξ_i^{-1}) such as to map the i^{th} LR image grid onto the HR grid.

In the update equation (6), the same step size μ^n is used for all color channels $(c = 1,2,3,4))$; this means that all the color channels are iteratively minimized at the same speed to avoid false coloring. The step size is calculated using the green component $(\overline{f}_G)$ according to the method of steepest

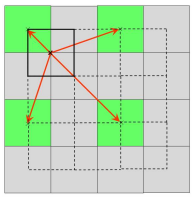

Figure 2: Pixel projection from interpolated RGB domain (dashed lines) onto a single raw color component (green 1). Note the uneven spacing that is used in the pixel projections.

descent [4] as follows:

$$\mu^n = \frac{1}{N}\sum_{i=1}^{N}\frac{||\overline{g}_{i(1)} - \mathbf{A}_{i(1)}\overline{f}_G^n||^2}{||\mathbf{A}_{i(1)}\overline{r}_{i(1)}^n||^2}. \quad (8)$$

4. IMPLEMENTATION

We recall that super-resolution algorithms involve several operations such as motion estimation, interpolation and downsampling. In the specific context of raw sensor images, we deal with multiple data channels corresponding to different spectral components (colors) as well as different temporal samples (images); this makes the alignment of all these data channels a challenging task that shall be carefully considered. In addition to the the proposed super-resolution method, the final image is ready after the image data undergoes a sequence of operations in the processing pipeline such as gaining, automatic white balancing, vignetting elimination, gamma correction, contrast enhancement, denoising, sharpening, etc. Most of these operations are specific to the sensor at hand, and in practice the combined efficiency of all these operations determine the final image quality. In the following however, we restrict the description to some specific aspects of the of the proposed method, and in the experiments we isolate the contribution of super-resolution only.

4.1 Motion estimation

One critical aspect in super-resolution is the need for accurate sub-pixel registration of the input images. In our implementation, we first used the subsampled color components to determine the 8 parameter geometry model corresponding to the global perspective with respect to a reference image. The parameters were estimated for each of the color channels separately and then further refined using a simple averaging operation to improve the accuracy.

Since the overall performance of super-resolution is particularly degraded in the presence of persistent outliers, we included a simple step to check if the mean square error (MSE) between the reference frame and the motion-compensated image is larger than a given threshold, if so, we skip that frame all together to avoid outliers.

4.2 Initialization of iterative super-resolution

Due to the absence of a proper regularization term, the iterative Least Squares solution that is described in equation (6) is prone to divergence especially when the number of input images is limited. To avoid this, we use a smooth initial estimate of the HR image and we limit the number of iterations. This may lead to a sub-optimal solution, however it also prevents annoying artifacts that could appear when over-iterated. The initial HR estimate is obtained by demosaicing the reference frame (the same that is used in the motion estimation) by applying simple bilinear interpolation of the color components, and then interpolating to the desired zoom factor in the RGB domain.

4.3 Projection functions

The image synthesis and the inverse process are defined respectively by $\mathbf{A}_{i(c)}$ and $\mathbf{W}_{i(c)}$. In our implementation, we used a method similar to that described in [7]. In the synthesis process, or the forward-projection, we warp the HR image as point samples and convolve them with a continuous form of the point-spread function (PSF) and we downsample at the required positions on the Bayer pattern. We assumed the PSF can be approximated with a Gaussian function so that we can easily integrate the blurring as a single parameter in the convolution process. Fig. 2 shows an example of the overlaid position of the HR image grid (in dashed line) with respect to the LR image grid. The corresponding half pixel shifts need to be integrated in the motion parameters of each LR image. The inverse operation, or the back-projection step $(\mathbf{W}_{i(c)})$ is handled in a similar manner. The region of influence that is used to calculate the back-projected pixel is determined by the interpolation filter, i.e., a small variance of the psf filter will require a small region of influence and will result in a sharper estimate; however this also means that more LR samples (N) are needed to avoid amplification of the noise and annoying pixelized artifacts in the solution. A smoother interpolation filter will make a compromise between the number of input images, the noise level and the sharpness of the result.

4.4 Processing the green channel

Another problem that we need to consider is that for each LR image we have 2 sub-images corresponding to the green color component, $\overline{g}_{i(1)}$ and $\overline{g}_{i(4)}$, and which correspond to a single channel in the HR image $(\overline{f}_G)$. This can be handled in many ways, for example by averaging the corresponding back-projected components, i.e., the residual gradients $\overline{r}_{(1)}^n$ and $\overline{r}_{(4)}^n$ due to the green spectral component; this solution has been used in the experiments presented in the following section. Alternatively, it is possible to use one of the channels for the regularization of the iterative solution, meaning that while $\overline{g}_{i(1)}$, $\overline{g}_{i(2)}$ and $\overline{g}_{i(3)}$ components of the Bayer image are used as reconstruction constraints of the G, R and B color components respectively, $\overline{g}_{i(4)}$ may be used as smoothness constraint of the final solution, especially if we assume a MAP iterative implementation, in this case $\overline{g}_{i(4)}$ can be used to calculate a non-redundant prior distribution of the HR image.

5. EXPERIMENTAL RESULTS

In this section, we describe experiments on synthetic and on real sensor data. First, we tested the algorithm on a sequence of synthetic test images. The images, 6 in total, were generated from a single HR image according to the imaging model described in equation (1). The original HR image was randomly warped using an 8 parameter projective model. We used a continuous Gaussian PSF ($\sigma_{psf}^2 = 1.5$) as the blurring

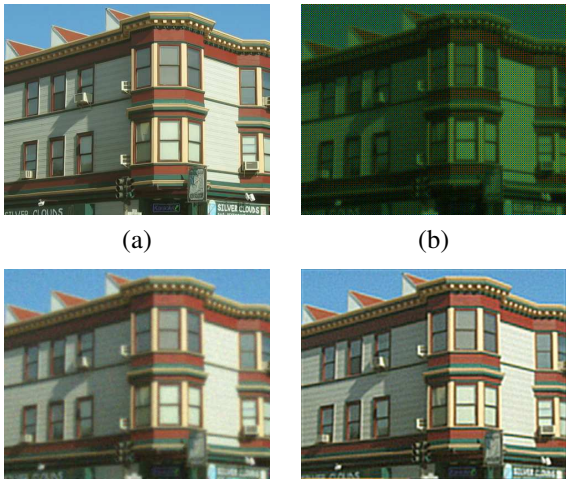

(a) (b) (c) (d)

Figure 3: (a) Original HR image. (b) Example LR image obtained according to model in equation (1), Gaussian PSF ($\sigma^2_{psf} = 1.5$), zoom factor 2, additive Gaussian noise ($\sigma^2 = 20$). (c) Image obtained using bilinear CFAI and zoomed to target size (2) using bicubic interpolation ($SNR_R = 9.44$, $SNR_G = 10.77$, $SNR_B = 10.45$, $SNR_Y = 10.19$). (d) Image obtained using the proposed algorithm, 2 iterations, ($SNR_R = 10.88$, $SNR_G = 12.19$, $SNR_B = 11.68$, $SNR_Y = 11.50$).

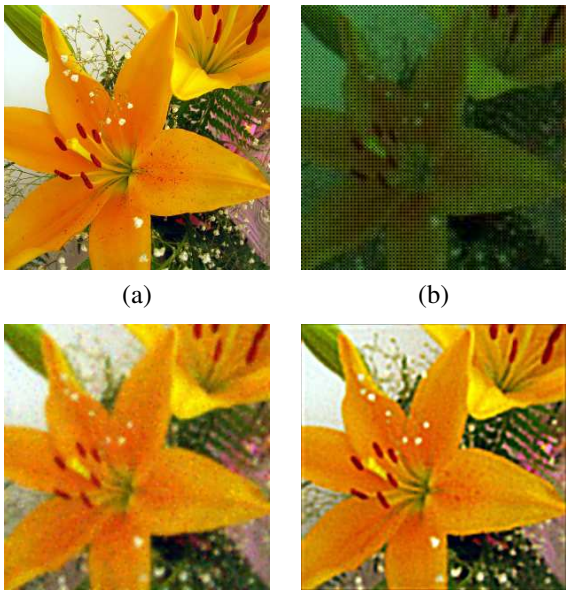

(a) (b) (c) (d)

Figure 4: (a) Original HR image. (b) Example LR image obtained according to model in equation (1), Gaussian PSF ($\sigma^2_{psf} = 2.5$), zoom factor 2, additive mixed noise (Gaussian noise $\sigma^2_\eta = 20$, impulsive noise $p = 0.06$). (c) Image obtained using bilinear CFAI and zoomed to target size (2) using bicubic interpolation ($SNR_R = 9.5$, $SNR_G = 9.43$, $SNR_B = 10.12$, $SNR_Y = 9.21$). (d) Image obtained by applying super algorithm (median fusing), 4 iterations, ($SNR_R = 10.92$, $SNR_G = 11.22$, $SNR_B = 12.16$, $SNR_Y = 11.19$).

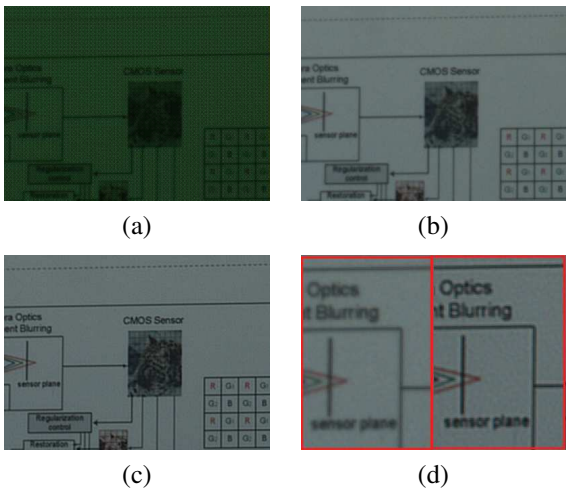

(a) (b) (c) (d)

Figure 5: (a) Example of raw data captured (4 images) with Micron test camera board (MI SOC1310). (b) Image obtained using bilinear CFAI interpolation of reference image. (c) Image obtained by applying proposed algorithm, zoom factor 1, 3 iterations. (d) Close-up comparison between zoomed portions of the images shown in (b) and (c).

operator, and we down-sampled the images by 2 to obtain the 6 LR images. We added to all input images a zero-mean Gaussian noise with variance $\sigma^2_\eta = 20$. Fig. 3 (c) shows the image that is demosaiced using bilinear CFAI interpolation and interpolated to target size (by 2) using bicubic interpolation. Fig. 3 (d) shows the result image that is obtained using the proposed algorithm after 2 iterations. For the images in (c) and (d), we calculated the signal to noise ratio with respect to the original image in (a) corresponding to the RGB color channels (SNR_R, SNR_G and SNR_B), and also for the luminance component (SNR_Y). These are shown in the caption of Fig. 3. In terms of *SNR*, the proposed super-resolution algorithm improves about $1.5db$ over equivalent traditional processing, i.e. applying separately the CFAI interpolation and resizing operation (bicubic interpolation). In addition, close visual inspection of the images in (c) and (d) confirms the superior results of the proposed algorithm as some fine details of the original image can be seen in the super-resolved image in (d) but are not visible when using a single image (c). The perceived image quality is also improved, since the contrast is enhanced and the colored artifacts due to noise are reduced. It is worth mentioning that the algorithm is relatively fast, for example in Fig. 3, the target image size was 320×240, and in this setting, the resulting images were computed in real-time on an ordinary PC.

In Fig. 4, we perform a similar experiment as above with different burring and noise parameters. 4 LR images were generated from a single HR image by random warp. We used a continuous Gaussian PSF ($\sigma^2_{psf} = 2.5$) and a down-sampling factor of 2. A mixture of Gaussian noise ($\sigma^2_\eta = 20$) and impulsive noise ($p = 0.06$) is added to all LR images. The aim is to emulate random noise that may appear in CMOS sensed images. Fig. 4 (c) shows the reference image that is demosaiced using bilinear CFAI interpolation and interpolated to target size (by 2) using bicubic interpolation. Fig. 4 (d) shows the result image that is obtained using the

proposed algorithm after 4 iterations. One simple modification with respect to earlier results is that in equation (7) we used the median filter instead of averaging filter, the idea is to account for impulsive noise present in the LR images. In terms of *SNR*, the super-resolved image is about $2db$ better than the image obtained using equivalent traditional processing, in particular the super-resolved image has less false coloring artifacts that are due to impulsive noise in the individual color components. This result is interesting because it shows that it is relatively easy to account for other types of spatial noise (in this case impulsive) by modifying the fusing step of the super-resolution algorithm, this result may be further developed in future work to account for other types of noise distributions.

In Fig. 5, we show the performance of the proposed method using real sensor data without prior knowledge of the distortion or motion that happened between the LR images. The proposed algorithm is applied on a set of 4 images captured by a CMOS camera board (Micron SOC1310). The images were taken slightly out-of-focus to simulate a fixed-focus optical system. In Fig. 5 (d), we show a zoomed portion of the image to compare the results obtained by applying simple bilinear interpolation against the images obtained using the proposed algorithm. Although the parameters that were used in our algorithm were tuned without accurate knowledge of the forward imaging model; the obtained results were good, i.e., by visual inspection it is clear that the details became sharper, the noise was decreased and the contrast in the super-resolved image was better. This confirms the usability of the proposed solution for practical application in camera systems.

6. CONCLUSIONS

In this paper, we presented a super-resolution algorithm that takes a sequence of raw color images and produces a demosaiced and zoomed color image in the RGB domain. The obtained results confirm the potential of this technique and its applicability for instance in a distinct multi-shot camera mode. In future work, we shall validate our method against an extensive set of known demosaicing algorithms to confirm the improvement in reproduction of color and detail resolution. Another interesting approach is to investigate different fusing methods that may be more appropriate to use in different noise environments of the sensors. Also, we shall consider the development of fast motion estimation techniques that are essential for similar applications.

REFERENCES

[1] T. Huang, R. Tsai, "Multi-Frame Image Restoration and Registration", *Advances in Computer Vision and Image Processing*, vol. 1, pp. 317-339, 1984.

[2] J. E. Adams Jr., "Design of practical color filter array interpolation algorithms for digital cameras", *Proc. SPIE* vol. 3028, pp. 117125, Feb. 1997.

[3] R.C. Hardie, K. Bernard and E. Armstrong, "Joint MAP Registration and High-Resolution Image Estimation Using a Sequence of Undersampled Images", *IEEE Transactions on Image Processing*, vol. 6, pp. 1621-1632, 1997.

[4] Bertero M., Boccaci P., *Inverse Problems in Imaging*, Chap. 6, Institute of Physics Publishing, Bristol, 1998.

[5] R. Kimmel, "Demosaicing: Image reconstruction from CCD samples", *IEEE Trans. Image Processing*, vol. 8, pp. 12211228, 1999.

[6] A. Blanksby and M. Loinaz, "Performance Analysis of a Color CMOS Photogate Image Sensor", *IEEE Transactions on Electron Devices*, vol. 47, no. 1, pp. 55-64, Jan. 2000.

[7] D. Capel, A. Zisserman, "Super-resolution Enhancement of Text Image Sequences", *Proceedings of the International Conference on Pattern Recognition (ICPR'00)*, Vol. 1, pp. 1600-1605, 2000.

[8] B. Gunturk, Y. Altunbasak, and R. M. Mersereau, "Color plane interpolation using alternating projections", *IEEE Transactions on Image Processing*, vol. 11, no. 9, pp. 997-1013, Sep. 2002.

[9] O. Kalevo and H. Rantanen, "Sharpening methods for images captured through Bayer matrix", *In Proc. IS&T-SPIE, Sensors, Cameras and Applications for Digital Photography V*, Vol. 5017, pp. 286-297, Jan. 2003.

[10] S. Park, M. Park, M. Kang, Super-Resolution Image Reconstruction: A technical Overview. *IEEE Signal Processing Magazine*, Vol. 20, pp. 21-36, 2003.

[11] S. Farsiu, M. Elad and P. Milanfar, "Multi-Frame Demosaicing and Super-Resolution from Under-Sampled Color Images", *Proceedings of the SPIE Conference on Computational Imaging*, vol. 5299, pp. 18-22, Jan. 2004.

[12] R. Lukac, K. Martin, and K.N. Plataniotis, "Digital Camera Zooming Based on Unified CFA Image Processing Steps", *IEEE Transactions on Consumer Electronics*, Volume 50, pp. 15-24, Feb 2004.

[13] T. Gotoh and M. Okutomi, "Direct Super-Resolution and Registration Using Raw CFA Images", *Proc.IEEE Computer Society Conference on Computer Vision and Pattern Recognition (CVPR04)*, vol. 2, 600-607, 2004.

[14] M. Shimizu, T. Yano and M. Okutomi, "Super-resolution under image deformation", *Proceedings of the IEEE Conference on Pattern Recognition*, Vol. 3, pp. 586-589 , August 2004.

[15] M. Trimeche, D. Paliy, M. Vehvilainen and V. Katkovnic, "Multichannel image deblurring of raw color components" *Proc. IS&T SPIE Electronic Imaging: Computational Imaging*, vol. 5674, pp. 169-179, Jan. 2005.

[16] B. Gunturk, J. Glotzbach, Y. Altunbasak, R. Schafer and R. Mersereau, "Demosaicking: color filter array interpolation", *IEEE Signal Processing Magazine*, Vol. 22, pp. 44-54, Jan. 2005.

[17] M. Trimeche, R.C. Bilcu and J. Yrjänäinen, "Adaptive Outlier Rejection in Image Super-resolution", *Eurasip Journal on Applied Signal Processing (JASP)*, Article ID 38052, Jan. 2006.

[18] P. Vandewalle, K. Krichane, D. Alleysson and S. Süsstrunk, "Joint Demosaicing and Super-Resolution Imaging from a Set of Unregistered Aliased Images", *Proc. IS&T SPIE Electronic Imaging: Digital Photography III*, Vol. 6502, 2007.